Finite element analysis of levee stability for flood early warning systems

Melnikova, N.B.

Publication date
2014

Chapter 4 Livedike case study: simulation and validation of the fluid sub-model[3]

The first validation of the *Virtual Dike* module was performed for the LiveDike - an earthen levee protecting a sea-port in Groningen, the Netherlands. The LiveDike was one of the research sites of the *UrbanFlood* project.

Besides the Livedike analysis, in this chapter we focus on the influence of variation in soil diffusivity on the pore pressure distribution. Correct calculation of pore pressures in the dike is critical for correct assessment of dike safety margin (it will be brightly illustrated on the example of another dike simulation – Boston levee validation site, Chapter 5). We did not analyze sensitivity of safety margin to soil strength parameters variation because there have been published many studies confirming that the safety margin is extremely sensitive to such variation (see, e.g., Griffiths and Lane, 1999). On the base of sensitivity analysis, we have constructed and implemented a new automatic procedure for calibration of soil diffusivities in an arbitrary heterogeneous dike based on historical pore pressure sensors recordings. The procedure has been successfully tested for the LiveDike diffusivities calibration.

LiveDike has been equipped with the Geobeads pore pressure sensors by Alert Solutions, measuring tidal fluctuations in real-time mode at the Livedike dashboard site http://livedijk-www.ict.tno.nl/, and at the Alert Solutions dashboard http://datapanel.alertsolutions.nl/asview/ (the sensor data are available for internal users only). Pore pressure readings were used to validate the fluid sub-model of the Virtual Dike module, by matching sensor data and simulated data and calibrating diffusivities of soil strata.

Realistic modelling of water flow through the dikes is necessary for correct estimation of effective stresses in the dikes and hence for predicting their stability. Calibration of diffusivities for the tidal groundwater flow is often performed by tidal methods (Smith and Hick, 2001), (Slooten et al., 2010), (Williams et. al., 1970) based on one-dimensional analytical models of semi-infinite or finite aquifers. This method is suitable for aquifers with nearly horizontal phreatic surfaces. A more accurate way that works well for high amplitude of water level variation is direct numerical simulation. In the present work, both analytical and numerical approaches have been tested and compared. Calibration of diffusivities of soil strata has been performed by matching tidal pore pressure fluctuations obtained from numerical simulation and from piezometers installed in several cross-sections of the dike. For heterogeneous soil structures, some averaged and simplified yet heterogeneous soil build-ups have been obtained, so that the response of the dike to the tidal load corresponds well to sensor measurements.

[3] Parts of this chapter have been published in (Melnikova, N.B., Krzhizhanovskaya, V.V., Sloot, P.M.A. (2013). Modelling Earthen Dikes Using Real-Time Sensor Data. Journal of Hydrology 496 (2013), pp. 154-165. DOI: 10.1016/j.jhydrol.2013.05.031)

4.1 LiveDike: geometry, soil build-up, loadings and sensor data

Livedike location and the view of the levee are shown in Figure 4-1a,b. The height of the dike is 9 m, the width is about 60 m and the length is about 800 m. The dike has a highly permeable sand core covered by a 60 cm thick clay layer.

The Livedike is a heterogeneous sand dike with clayey inclusions and gentle slopes (14° and 18° for the sea side and the land side slopes, respectively). Typical value of angle of internal friction for sand lies in the range of 25°-30°; this lets to conclude that macro-instability does not threat to the dike safety.

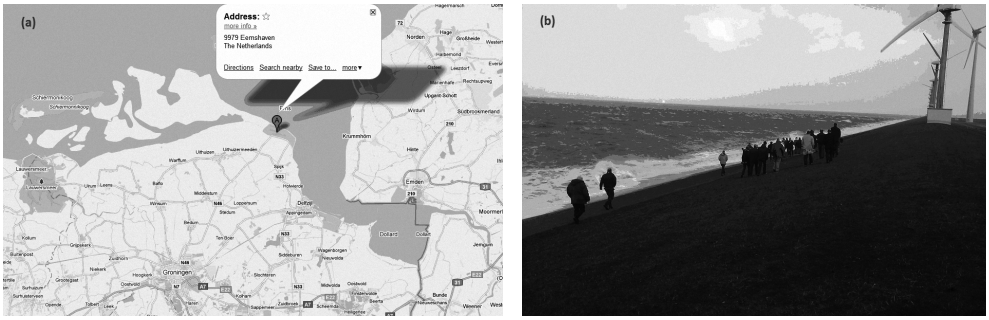

Figure 4-1 (a) LiveDike: (a) location of the test site near Groningen, The Netherlands; (b) photo of the dike

The LiveDike has been equipped with sensors with GPS locations shown in Figure 4-2a. Sensors are placed in four cross-sections (slices), see Figure 4-2a,b. These slices have been simulated in 2D models under tidal water loading, in order to calibrate diffusivities, simulate flow through the dike and finally analyze the structural stability of the dike.

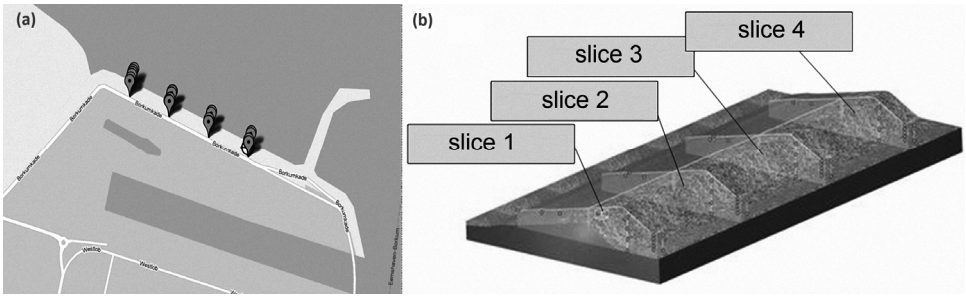

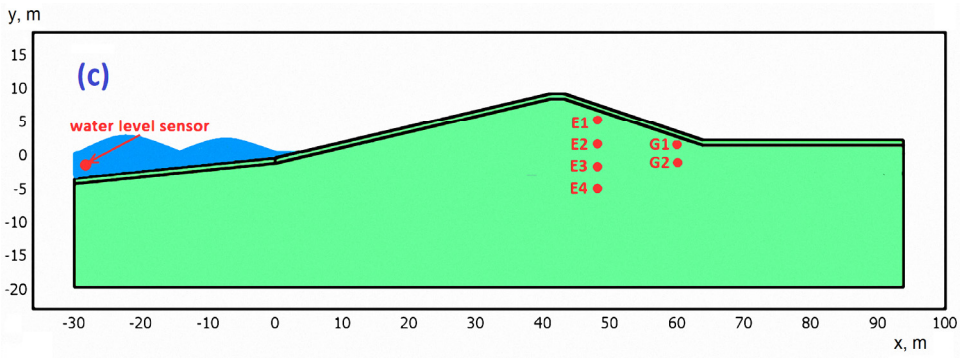

Figure 4-2 (a) Top view at the LiveDike (Eemshaven); (b) Slices of the LiveDike; (c) 2D model of a dike slice with pore pressure sensor locations shown with red dots

A geometric model of a dike slice with sensor locations is presented in Figure 4-2c. Sensors E1-E4 and G1-G2 measure absolute pore pressure and temperature and produce data stream which is available in real-time on web dashboards. For calibration of the model, we used signals from the E3, E4 and G2 pore pressure sensors located below the phreatic surface. An input signal for simulation was the water level registered by the sensor installed outside of the dike. The sea-side toe of the dike is located at x=0 m, y=-0.7 m, while the mean sea level is at y=0 m.

The soil build-up for a longitudinal cross-section passing through the crest of the dike is presented in Figure 4-3. It contains horizontal layers of sand (1 - light orange), silty sand with small clay inclusions (5 - lemon) and 60 cm clay layer that covers the dike (2 - blue). Grey areas (4) are clayey sand. Below the sand layers lies impermeable clay layer (3 - blue). Cone penetration test (CPT) results (cone end resistance and frictional resistance) are schematically shown with black lines. More information on the CPT testing methodology can be found in (Meigh, 1987).

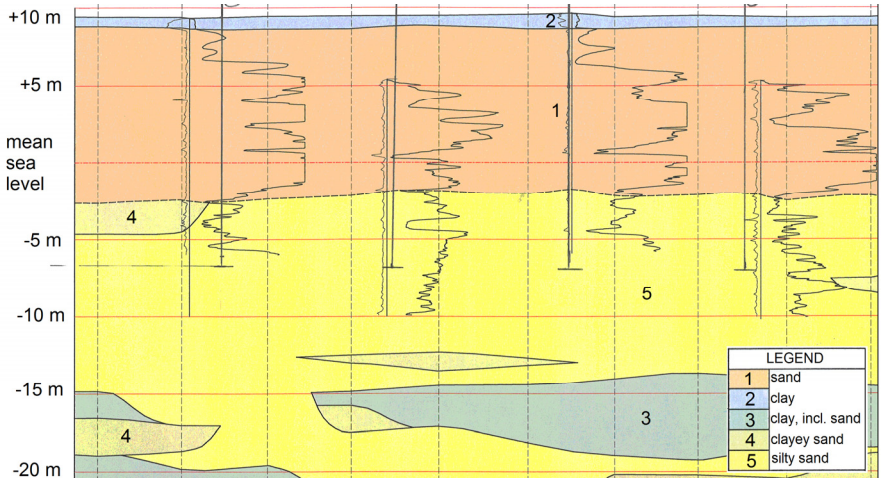

Figure 4-3. Soil build-up in the LiveDike and underlying soil strata

A sample of sensor data showing air pressure, sea level and pore pressure is presented in Figure 4-4 and Figure 4-5, for a time period that has been used for diffusivity calibration ("training period"). Sea level dynamics is presented in Figure 4-4b, with positions of local maximum and minimum marked with dashed lines. Figure 4-5 presents pore pressure measured in three slices of the dike. For calibration of diffusivities, the original pore pressure signals were smoothed (denoised) by a localized linear fit algorithm with an adaptive window (the smoothed signals are also shown in Figure 4-5). Then the levels of minimal and maximal tidal pressure were detected for the smoothed pressure signals. These levels are shown in Figure 4-5 with horizontal dashed lines. Corresponding pressure values are specified in the legends. Vertical dashed lines show the moments in time corresponding to the minimal and maximal pressure values. The corresponding time values are specified in the legends. The obtained relative pressure amplitudes and time delays between local pressure maximum and sea level maximum are presented in Table 4-1 (page 37).

E3 and E4 sensors are located at the same distance from the sea (x=50 m), but at the different levels (y=-1.5 m and y=-5.5 m from the reference level, correspondingly). E3 pressure oscillations are lower than E4 oscillations and this fact points to the presence of a vertical heterogeneity in the dike. A time delay between E4 oscillations (at x=50 m) and tidal oscillations (at x=0 m) varies in the range between 3 and 18 min, which indicates highly permeable sand in the zone 0 <x<50 m. E3 oscillations lag from tidal oscillations by 9-38 min.

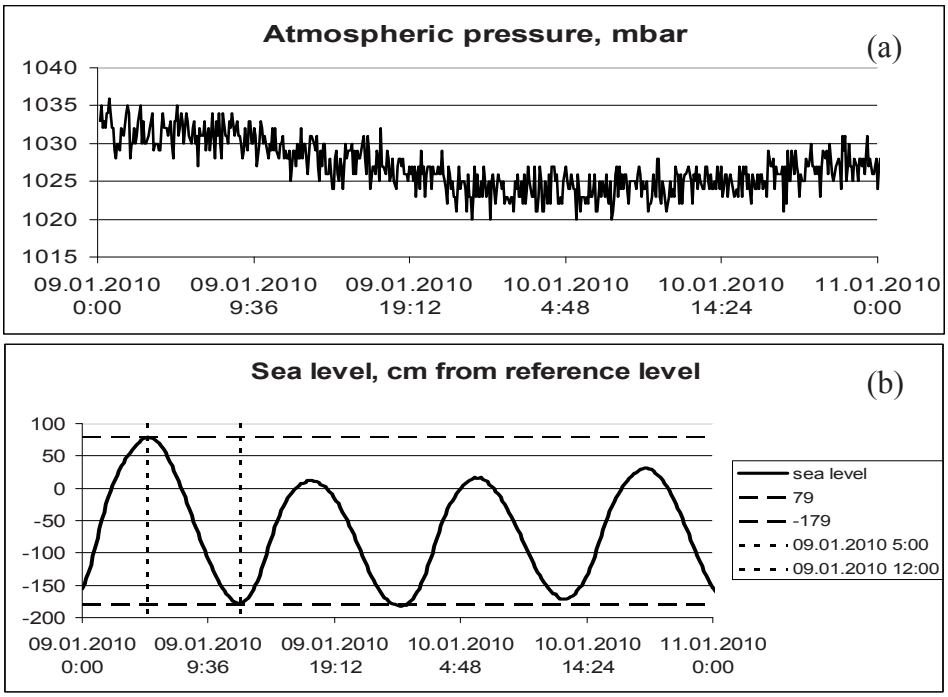

Figure 4-4. LiveDike: (a) atmospheric pressure [mbar] and (b) sea level [cm] registered by sensors

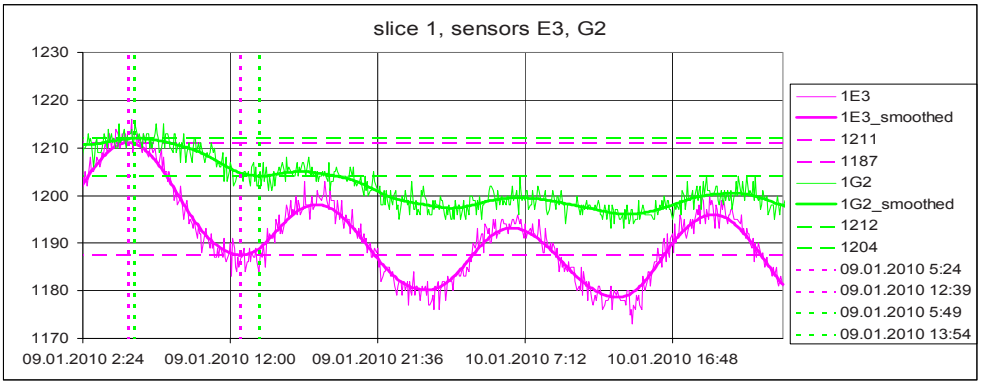
slice 1, sensors E3, G2
1230
1220
1210
1200
1190
1180
1170
09.01.2010 2:24
09.01.2010 12:00
09.01.2010 21:36
10.01.2010 7:12
10.01.2010 16:48
1E3
1E3_smoothed
1211
1187
1G2
1G2_smoothed
1212
1204
09.01.2010 5:24
09.01.2010 12:39
09.01.2010 5:49
09.01.2010 13:54

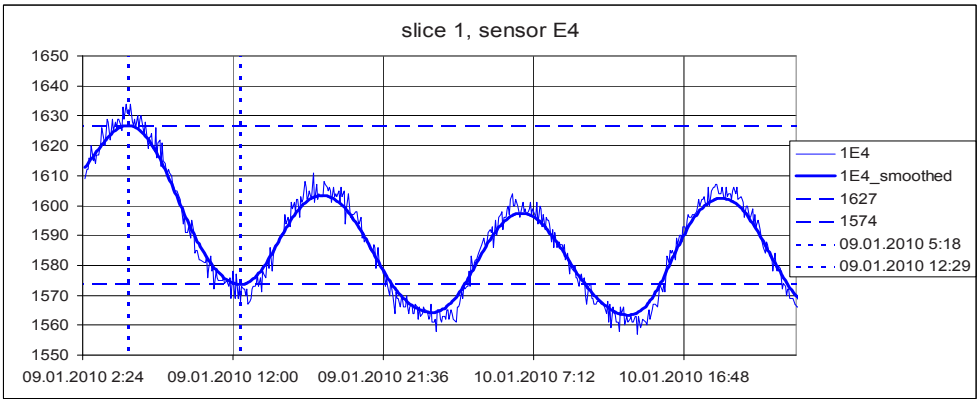
slice 1, sensor E4
1650
1640
1630
1620
1610
1600
1590
1580
1570
1560
1550
09.01.2010 2:24
09.01.2010 12:00
09.01.2010 21:36
10.01.2010 7:12
10.01.2010 16:48
1E4
1E4_smoothed
1627
1574
09.01.2010 5:18
09.01.2010 12:29

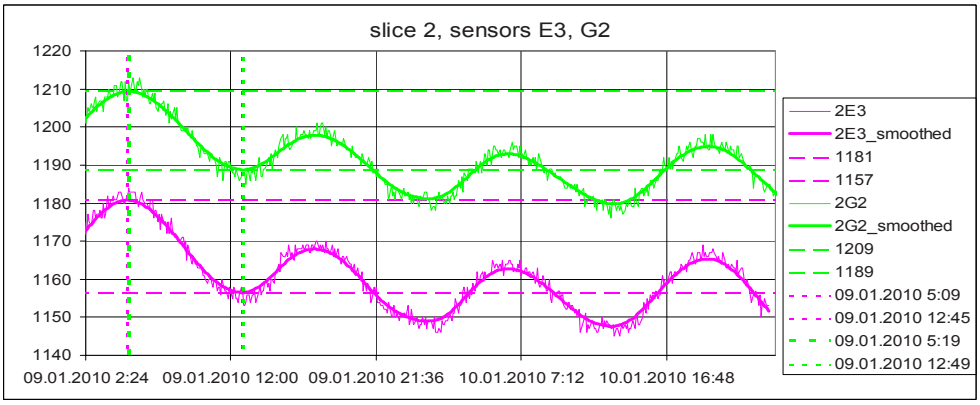
slice 2, sensors E3, G2
1220
1210
1200
1190
1180
1170
1160
1150
1140
09.01.2010 2:24
09.01.2010 12:00
09.01.2010 21:36
10.01.2010 7:12
10.01.2010 16:48
2E3
2E3_smoothed
1181
1157
2G2
2G2_smoothed
1209
1189
09.01.2010 5:09
09.01.2010 12:45
09.01.2010 5:19
09.01.2010 12:49

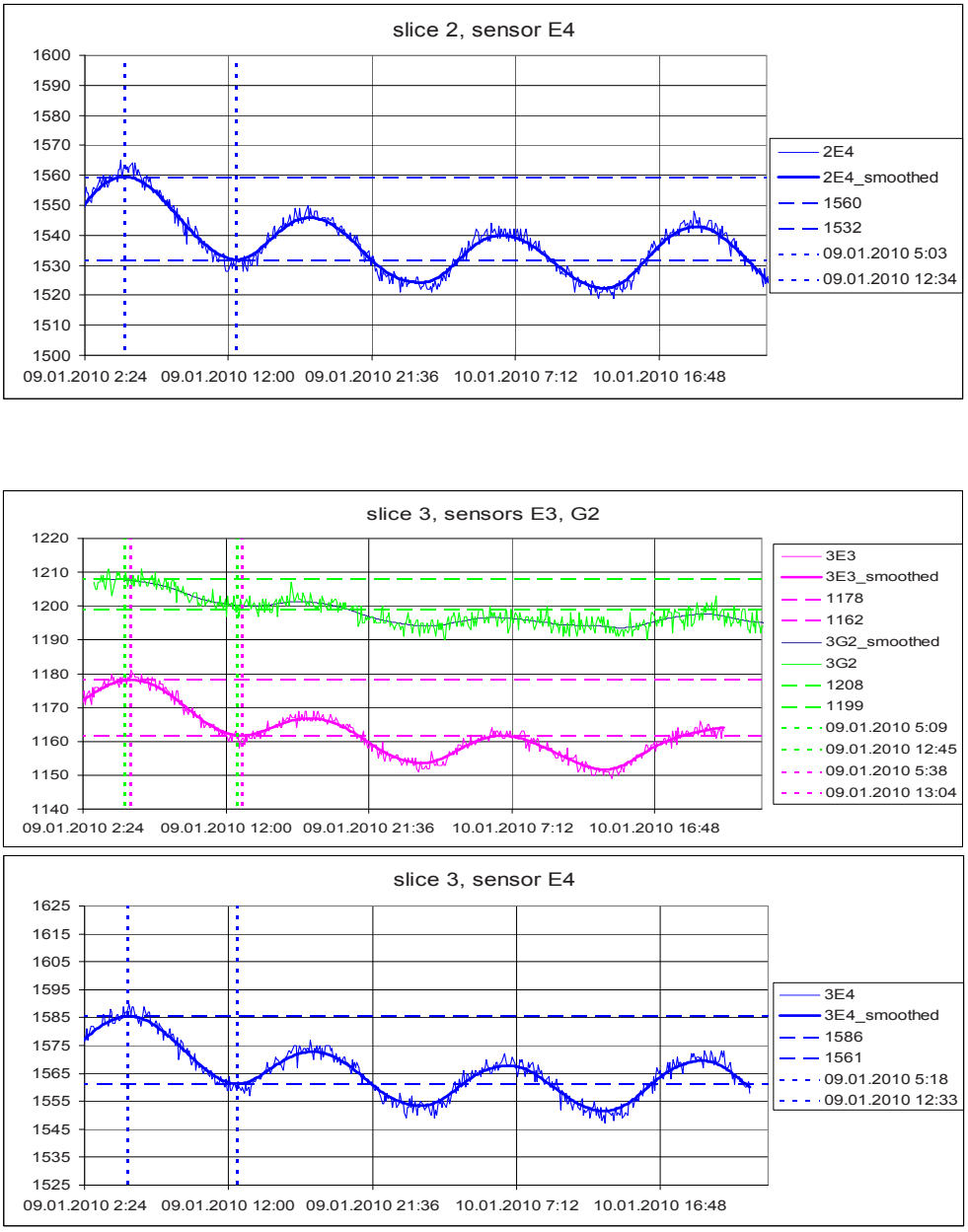

Figure 4-5. LiveDike: absolute pore pressure [mbar] registered by sensors and smoothed pressure signals

E3 and G2 sensors are located at approximately the same level (-1.2 m÷-1.5 m from ref. level), but at different distances from the sea (x=50 and x=62 m, correspondingly). In the first slice, the amplitude of pore pressure dissipates quickly within 12 m of horizontal distance between E3 and G2 sensors (Table 4-1). It indicates the presence of a horizontal

heterogeneity in the sand layers, with diffusivity decreasing with the distance from the sea, up to a dense impermeable zone near G2. This impermeable zone creates high time lag between G2 oscillations and tidal oscillations: the lag equals to 49 min in the first slice.

Table 4-1. LiveDike pressure sensors measurements: relative pressure amplitudes and time delays between the tide and local pressure fluctuations

Sea water level sensor data						
sea level drop: 258 cm = 253 mbar; time of local maximum: 9.01.2010 5.00						
Pore pressure sensors data						
	Slice1	Slice2	Slice3	Slice1	Slice2	Slice3
	Relative daily oscillations amplitude (fraction of tidal daily oscillations amplitude)			Time delay between local pressure maximum and sea level maximum, minutes		
E4	0.21	0.11	0.10	18	3	18
E3	0.09	0.10	0.07	24	9	38
G2	0.03	0.08	0.04	49	19	9

In order to reproduce the actual pore pressure fluctuations, a heterogeneous 2D model of the 1st slice of the LiveDike was built. Below we present the mathematical model of porous flow, numerical and analytical studies of diffusivity influence on the pore pressure dynamics in the dike and calibration of diffusivities based on sensor data.

4.2 Governing equations, model data and computational mesh

Water flow through the dike was modelled by Richards' equation (2.12) with the van Genuchten model (2.4)-(2.6) for water retention in partially saturated soil around the phreatic surface. The boundary conditions are shown in Figure 4-6:

magenta boundaries are walls with zero normal flux $\frac{\partial p}{\partial n} = 0$;

black boundaries are sea side with tidal pressure oscillations specified:

$$\begin{cases} p = \rho g \cdot (h(t) - y) \quad for \quad y \le h(t) \\ p = 0 \quad for \quad y > h(t) \end{cases}, \tag{4.1}$$

where *h(t)* is oscillating sea level [m], measured by sensors or predicted by hydrological model;

blue boundaries are land side with attenuated oscillations of ground water level:

$$\begin{cases} p = \rho g \cdot (h_{gw}(t) - y) \quad for \quad y \le h_{gw}(t), \\ p = 0 \quad for \quad y > s(t) \end{cases}, \tag{4.2}$$

where $h_{gw}(t)$ denotes oscillating ground water level, representing attenuated and altered tidal signal.

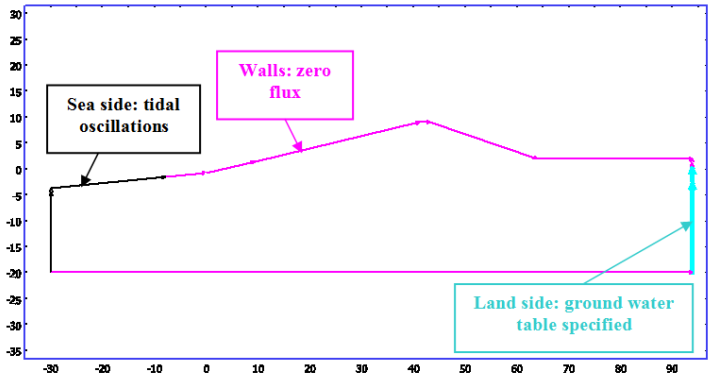

Figure 4-6. 2D simulation domain and boundary conditions

In the regime of forced tidal oscillations, the initial condition in (2.12) does not affect the steady solution, due to dissipation of the initial pore pressure distribution within several tidal periods. A hydrostatic distribution below y=0 m was specified as a technical initial condition, like it was described in section 2.1.3.

In the saturated zone, where θ_e=1, C=0, k_r=1, porous flow is modelled by linear and parabolic Laplace equation:

$$\frac{\partial p}{\partial t} + \nabla \cdot [-d \nabla (p + \rho g y)] = 0 \,, \tag{4.3}$$

where $d = K_S / S\mu$ [m^2/s] is soil-water diffusivity, the only soil parameter that influences pore pressure dynamics under the specified load.

Table 4-2 gives a list of soil parameters that define unsaturated behaviour and strength/stiffness characteristics of soil. These parameters have been set for the LiveDike using reference properties of sand.

Table 4-2. LiveDike – soil parameters

Van Genuchten parameters			Young's modulus E, Pa	Poisson's ratio ν	Friction angle φ, degrees	Cohesion c, Pa
α, [1/m]	n	l				
8	1.5	0.5	10^{10}	0.3	30	0

Water viscosity is calculated as a linear interpolation function of water temperature between the points defined in Table 4-3. Figure 4-7 shows water temperature measurements over a period of one year. Due to the variation of water viscosity, the value of soil diffusivity in summer is 1.8 times higher than in winter.

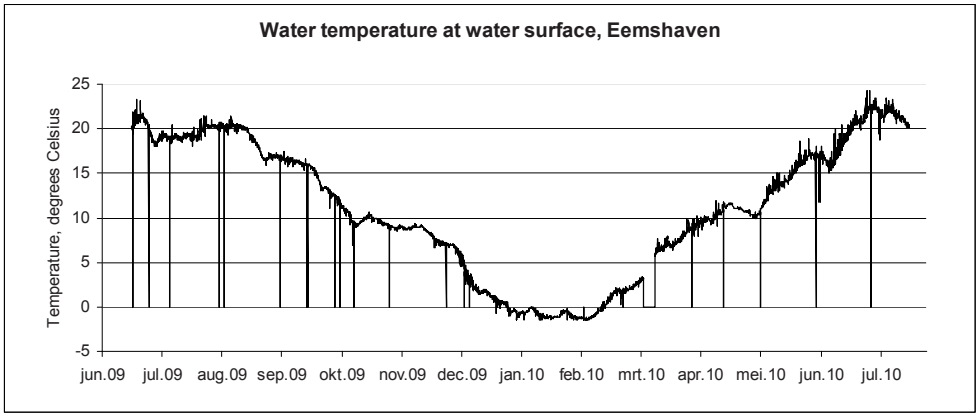

Figure 4-7. Sea water temperature distribution during year cycle

Table 4-3. Water viscosity values

Temperature, ^{o}C	Dynamic viscosity, Pa·s
20	$1.004 \cdot 10^{-3}$
10	$1.307 \cdot 10^{-3}$
0	$1.797 \cdot 10^{-3}$

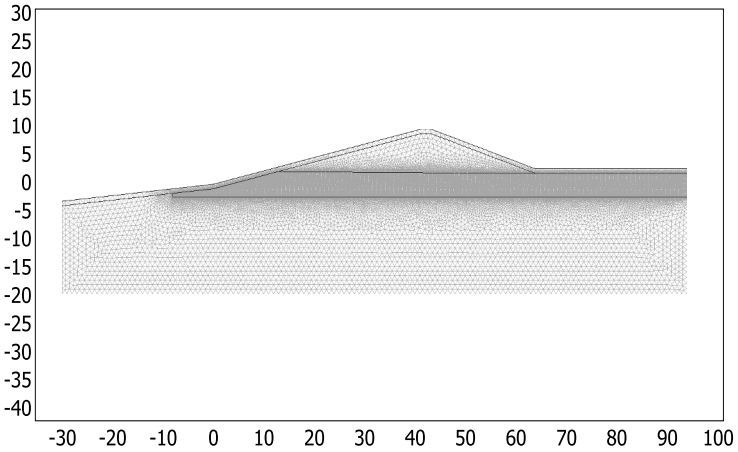

Figure 4-8. Livedike: finite element mesh with refinement zone around the phreatic line

Finite element mesh used for all computations (for both sensitivity analysis and Livedike calibration parameters) was composed from triangular elements of second order of

space approximation (Figure 4-9). The mesh contains refinement zone located around the phreatic line (which changes its shape during tidal oscillations), where pressure gradient is high. The total number of elements is about 15000.

4.3 2D numerical sensitivity analysis of pressure amplitude and time delay to the variation of soil diffusivity

Sensitivity analysis has been performed to study the influence of saturated soil-water diffusivity on tidal oscillations of pore pressure in the dike. A 2D homogeneous dike model has been considered. Geometric prototype of the model is the LiveDike slice. Boundary conditions' zones have been described in section 4.2. At the seaside, harmonic tidal pressure oscillations are specified; at the landside, the ground water level is constant (zero meters from average sea level). A number of porous flow simulations have been performed, with saturated diffusivities varied in the range of 0.1-1000 m^2/s. Distribution of relative pore pressure amplitudes, normalized to tidal amplitude, is presented in Figure 4-9a, for a horizontal slice of the dike (at the level y = -5.5 m).

For relatively high values of diffusivity ($d = 10 \div 1000\ m^2/s$) relative pressure amplitude distribution is linear with a very small non-linear tail close to the sea-side (left) slope. The non-linear part corresponds to the zone where the flow is essentially two-dimensional: at $x \leq 0$ m, water penetrates into the domain both through the vertical boundary and through the under-water slope of the dike (see Figure 4-10 for arrow plot of flow velocity). At $x \geq 0$ m the flow is almost one-dimensional, and relative pressure amplitude distribution qualitatively agrees with the 1D analytical solution presented in the next paragraph.

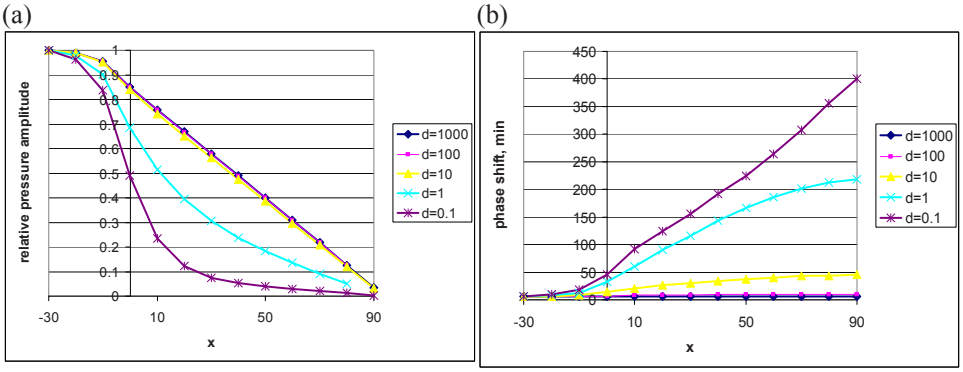

Figure 4-9. Numerical study of sensitivity of tidal oscillations to diffusivity variation, 2D analysis: (a) relative pressure amplitude distribution along the dike; (b) time delay distribution along the dike. Data shown in a horizontal slice y = - 5.5 m (at the level of the E4 sensor, see Figure 4-2(c))

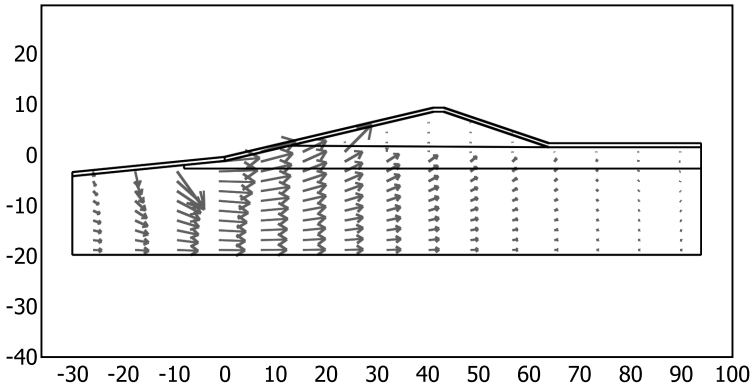

Figure 4-10. Arrow plot of velocity field (high tide). The flow is essentially two-dimensional at the sea bottom, x≤0 m

Figure 4-9a shows that, in a relatively short computational domain (~100 metres long) and for loose, permeable media (like gravel and coarse sand), simulated amplitude of tidal fluctuations is insensitive to the actual value of diffusivity (see lines for d=1000, d=100, d=10). This linear distribution is only defined by the amplitude of tidal fluctuations at the sea-side and at the land-side boundaries of the domain. To the contrary, time delay is sensitive to the value of diffusivity in the whole range (Figure 4-9(b)), therefore time delay can be calibrated by tuning diffusivity value.

For diffusivities d≤1 m^2/s, a significant non-linearity appears in the pressure amplitude distribution: pore pressure amplitude within the dike depends on the diffusivity.

Figure 4-11 shows pressure amplitude and time delay as functions of diffusivity, in LiveDike E4 sensor location (50;-5.5). The amplitude and phase delay values of E4 sensor are shown in Figure 4-11 with dashed lines.

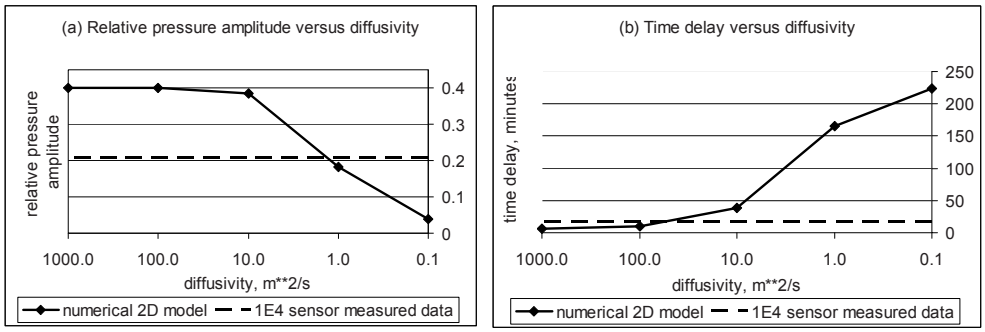

Figure 4-11. Numerical study of influence of soil diffusivity on: (a) relative pore pressure amplitude and (b) time delay in E4 sensor location (50m; -5.5m). Actual sensor readings shown with dashed lines

From Figure 4-11 it is clear that matching both the amplitude and phase lag with only one parameter (diffusivity) is impossible: matching the amplitude value requires

diffusivity d~1 m^2/s, while matching the time delay requires that d~100 m^2/s. Formally, besides the diffusivity, one more parameter (a length of a homogeneous zone in the layered soil build-up) is necessary to match the data for one sensor. In fact, this contradiction indicates presence of heterogeneity in the LiveDike soil build-up (while the prototype dike in sensitivity analysis is homogeneous). Thus we construct a model of a dike as a set of horizontal stripes, each stripe divided into a number of homogeneous sectors with constant diffusivity. The length of a sector is the second parameter necessary for matching sensor data (Figure 4-12). Figure 4-12 presents a scheme of construction of a heterogeneous dike model to match sensor data. Sensors E_1, E_2, G_1 are not taken into consideration in the model as they are located above the phreatic surface and they do not produce data on pore pressure. For 6 values to match (these are pressure amplitude and time delay for 3 sensors: E_4, E_3, G_2), 6 parameters have been used: lengths of homogeneous zones L_1, L_2 and diffusivities d_1, d_2, d_3, d_4 (see Figure 4-12). After calibration a total length of the simulation domain equals to the sum of parameters L_1, L_2.

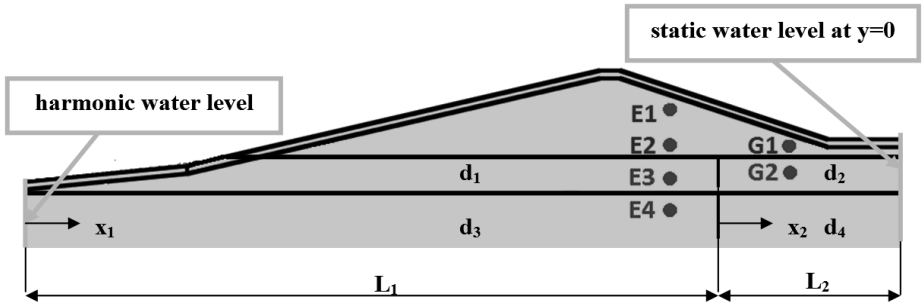

Figure 4-12. Construction of a heterogeneous dike model to match sensor data

4.4 1D analytical sensitivity analysis of tidal pressure oscillations to the variation of soil diffusivity

In this section, two analytical solutions for the problem of harmonic flow in a one-dimensional saturated homogeneous aquifer are derived and compared to the direct numerical solutions which were discussed above. A one-dimensional analytical model can be used for modelling tidal propagations through the aquifers with a low gradient of the phreatic line.

The objectives for employing one-dimensional analytical models for dike diffusivity calibration are:

- Obtaining formulas for initial guess values of diffusivity;
- Qualitative study of penetration of tidal waves through the dike

Flow in a one-dimensional saturated aquifer is described by the equation

$$\frac{\partial p}{\partial t} - d \cdot \frac{\partial^2 p}{\partial x^2} = 0\,, \tag{4.4}$$

Harmonic boundary conditions defining two different problems are considered:

- A semi-infinite aquifer with sine oscillations of water pressure at the boundary x=0:

$$\begin{aligned} &p(x,t)\big|_{x=0} = A\sin(\omega t) \\ &p(x,t)\big|_{x\to\infty} \to 0 \end{aligned}\,, \tag{4.5}$$

where A is amplitude of pressure oscillations; ω is angular frequency;

- A finite aquifer with sine pressure oscillations at x=L and constant pressure p=0 at x=0:

$$\begin{aligned} &p(x,t)\big|_{x=L} = A\sin(\omega t) \\ &p(x,t)\big|_{x=0} = 0 \end{aligned}\,, \tag{4.6}$$

Initial conditions for (4.4) are not considered here, as we are interested in the settled, tide-forced pressure oscillations. The settled solution for the semi-infinite aquifer problem (4.4) with boundary conditions (4.5) is expressed as follows (Ferris, 1951):

$$p(x,t) = Ae^{-x\sqrt{\frac{\omega}{2d}}} \cdot \sin\left[\omega(t - x\sqrt{\frac{1}{2d\omega}})\right], \tag{4.7}$$

It represents a wave of pore pressure travelling in compressible soil, with an amplitude p_A [Pa] dissipating exponentially with the distance from the inlet, and a time delay Δt [s] growing linearly with the distance:

$$p_A(x) = Ae^{-x\sqrt{\frac{\omega}{2d}}},\ \Delta t = x\sqrt{\frac{1}{2d\omega}} \tag{4.8}$$

Applying solution (4.7) to the model of the dike described in section 4.2 (for $-30 \le x \le 90$), we get distributions of relative pressure amplitude $p_A(x)/A$ and time delay Δt (in a logarithmic scale), presented in Figure 4-13a,b. Diffusivity d varied in the range between 0.1 and 1000 m^2/s. Tidal frequency ω=2π/T, where T=12 hrs 25 min.

Figure 4-13a gives an estimate for a distance at which tidal waves penetrate into a homogeneous aquifer. For dense impermeable soils with diffusivity d≤0.1, pressure amplitude dissipates to a level of 4% of tidal amplitude, within the distance of 120 meters

from the sea. For highly permeable soils with diffusivity $\geq 10 m^2/s$, pressure amplitude distribution is linear in the whole domain, and this linear distribution has been confirmed by the 2D numerical analysis (section 4.2).

According to formula (4.8), slow seasonal water table fluctuations propagate further into an aquifer than daily fluctuations do, and this was taken into consideration for the LiveDike when specifying land side boundary conditions in the porous flow problem (section 4.5).

For the finite aquifer problem (4.4) with boundary conditions (4.6), solution representing steady harmonic oscillations and satisfying zero boundary condition $p(x,t)\big|_{x=0} = 0$ can be expressed as a sum of two complex conjugated independent partial solutions of (4.4):

$$p = Ce^{i\omega t}\sinh(\sqrt{\frac{i\omega}{d}}x) + \overline{C}e^{-i\omega t}\sinh(\sqrt{-\frac{i\omega}{d}}x), \tag{4.9}$$

where $i = \sqrt{-1}$; $C = \mathrm{Re}(C) + i \cdot \mathrm{Im}(C)$ is a complex constant to be determined from the harmonic boundary condition:

$$p(x,t)\big|_{x=L} = A\sin(\omega t) \Leftrightarrow$$

$$\Leftrightarrow C(\cos(\omega t) + i\cdot\sin(\omega t))\sinh(\sqrt{i\frac{\omega}{d}}L) + \overline{C}(\cos(\omega t) - i\cdot\sin(\omega t))\sinh(\sqrt{-i\frac{\omega}{d}}L) = A\sin(\omega \tag{4.10}$$

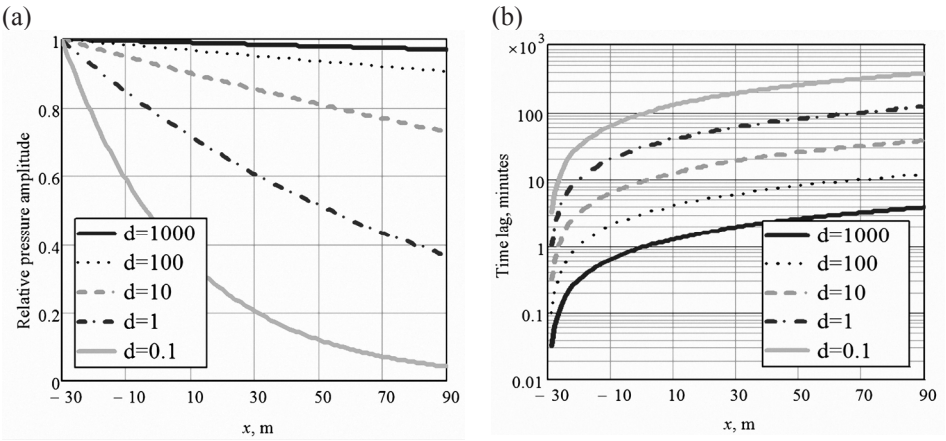

Figure 4-13. Analytical study of sensitivity of tidal oscillations to diffusivity variation, 1D model of a semi-infinite saturated aquifer: (a) relative pressure amplitude distribution along the domain; (b) time lag, minutes, along the domain – in a logarithmic scale

From (4.10) follows that:

$$C = \frac{A}{2i\sinh(\sqrt{i\frac{\omega}{d}}L)}, \tag{4.11}$$

(4.9)+(4.11) $\Rightarrow$

$$p(x,t)\Big| = 2\,\mathrm{Re}\left\{\frac{A\cdot\sinh(\sqrt{i\frac{\omega}{d}}x)}{2i\cdot\sinh(\sqrt{i\frac{\omega}{d}}L)}(\cos(\omega t)+i\cdot\sin(\omega t))\right\}, \tag{4.12}$$

Taking into account that

$$\sinh(\sqrt{\frac{i\omega}{d}}L) = \cos(\sqrt{\frac{\omega}{4d}}L)\sinh(\sqrt{\frac{\omega}{4d}}L) + i\cdot\sin(\sqrt{\frac{\omega}{4d}}L)\cosh(\sqrt{\frac{\omega}{4d}}L), \tag{4.13}$$

(4.12) can then be written as:

$$\begin{aligned} &p(x,d,L,t) = p_A(x)\cdot\sin(\omega(t-\Delta t)),\\ &p_A(x,d,L) = A\sqrt{\frac{\cosh(x\sqrt{\frac{\omega}{d}})-\cos(x\sqrt{\frac{\omega}{d}})}{\cosh(L\sqrt{\frac{\omega}{d}})-\cos(L\sqrt{\frac{\omega}{d}})}},\\ &\Delta t(x,d,L) = \begin{cases}\frac{1}{\omega}\cdot arctg\left[\frac{\exp r1}{\exp r2}\right] & if \quad \exp r2>0\\ \frac{1}{\omega}(\pi + arctg\left[\frac{\exp r1}{\exp r2}\right]) & otherwise\end{cases}, \end{aligned} \tag{4.14}$$

Here

$$\begin{aligned} \exp r1 &= -\sinh(\sqrt{\frac{\omega}{4d}}(x+L))\cdot\sin(\sqrt{\frac{\omega}{4d}}(x-L)) + \sinh(\sqrt{\frac{\omega}{4d}}(x-L))\cdot\sin(\sqrt{\frac{\omega}{4d}}(x+L)),\\ \exp r2 &= \cosh(\sqrt{\frac{\omega}{4d}}(x+L))\cdot\cos(\sqrt{\frac{\omega}{4d}}(x-L)) - \cosh(\sqrt{\frac{\omega}{4d}}(x-L))\cdot\cos(\sqrt{\frac{\omega}{4d}}(x+L)) \end{aligned} \tag{4.15}$$

Expression (4.14) describes distributions of relative pore pressure amplitude and oscillations' time lag along the bounded aquifer (see Figure 4-14 for their graphical representation).

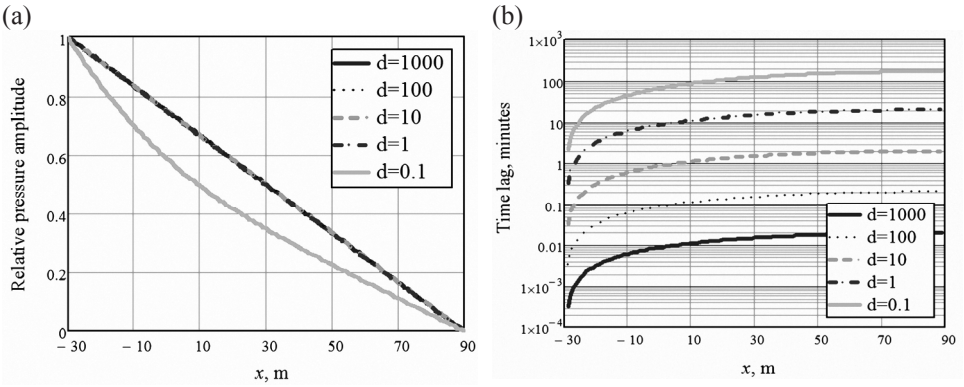

Figure 4-14. Analytical study of sensitivity of tidal oscillations to diffusivity variation, 1D model of a bounded saturated aquifer: (a) relative pressure amplitude distribution; (b) time lag, minutes– in a logarithmic scale

For dense soils with diffusivity d<=1 m^2/s, the analytical model predicts non-linear profiles of pressure distribution, however the absolute values of pore pressure do not agree with the 2D numerical simulation. For example, for d=1 m^2/s, analytical relative pressure amplitude in point x=50 m $P_A = 0.511$, while in the 2D numerical solution simulated amplitude $P_A = 0.2$.

Possible sources of mismatch between the two models are: two-dimensional flow behaviour at the sea-side and diffusion of water above the phreatic line, which is considered in the 2D numerical model only.

Calibration of the LiveDike soil parameters based on the sensitivity analysis is described in section 4.5.

4.5 Automatic procedure for diffusivities calibration

Calibration has been performed for the first slice of the dike. As it was mentioned in section 4.3, we have to find the values of 6 parameters: lengths of homogeneous zones L_1, L_2 and diffusivities d_1, d_2, d_3, d_4 (see Figure 4-12). Below we describe the procedure of diffusivity calibration using measured data from 3 sensors: E3, E4 and G2 (Figure 4-12). The algorithm is generic and can be used for any number of sensors in a dike slice.

Initial estimate values of L and d parameters are obtained by superposition of analytical solutions derived from the solution (4.14) for various periodic boundary conditions:

- In the 1st zone (d=d_1, 0<x_1<L_1): $p_1(x_1,t) = p_{11}(x_1,t) + p_{12}(x_1,t)$, where $p_{11}(x_1,t)$ is a solution of (4.4) with the boundary conditions:

$$p_{11}(x_1,t)\big|_{x_1=0} = A\sin(\omega t),\ p_{11}(x_1,t)\Big|_{x_1=L_1} = 0, \tag{4.16}$$

and $p_{12}(x_1,t)$ is a solution of (4.4) with the boundary conditions:

$$p_{12}(x_1,t)\big|_{x_1=0} = 0, p_{12}(x_1,t)\big|_{x_1=L_1} = A_{interface1}\sin(\omega t + \varphi_{interface1}), \tag{4.17}$$

Here A is tidal amplitude, ω is tidal frequency, $A_{interface1}$, $\varphi_{interface1}$ are local amplitude and phase delay on the interface of zones #1 and #2 (not known a priory, to be determined from a continuity condition (4.19);

- In the 2[d] zone ($d=d_2$, $0<x_2<L_2$): $p_2(x_2,t)$ is a solution of (4.4) with the boundary conditions:

$$p_2(x_2,t)\big|_{x_2=0} = A_{interface1}\sin(\omega t + \varphi_{inetrface1}), p_2(x_2,t)\big|_{x_2=L_2} = 0; \tag{4.18}$$

- Continuity condition for the interface between 1[st] and 2d zones states that the value of flow velocity does not change at the interface:

$$\frac{\partial}{\partial x_1} p_1(x_1,t)\Big|_{x_1=L_1} = \frac{\partial}{\partial x_2} p_2(x_2,t)\Big|_{x_2=0} \tag{4.19}$$

From equation (4.19), we obtain two independent conditions: one for oscillation amplitude $A_{interface1}$ and one for oscillation phase $\varphi_{interface1}$.

- In the 3[d] zone: ($d=d_3$, $0<x_1<L_1$): $p_3(x_1,t) = p_{31}(x_1,t) + p_{32}(x_1,t)$, where $p_{31}(x_1,t)$ is a solution of (4.4) with the boundary conditions:

$$p_{31}(x_1,t)\big|_{x_1=0} = A\sin(\omega t), p_{31}(x_1,t)\big|_{x_1=L_1} = 0 \tag{4.20}$$

$p_{32}(x_1,t)$ is a solution of (4.4) with the boundary conditions:

$$p_{32}(x_1,t)\big|_{x_1=0} = 0, p_{32}(x_1,t)\big|_{x_1=L_1} = A_{interface2}\sin(\omega t + \varphi_{interface2}), \tag{4.21}$$

where $A_{interface2}$, $\varphi_{interface2}$ are unknown local amplitude and phase delay on the interface of zones #3 and #4;

- In the 4[th] zone ($d=d_4$, $0<x_2<L_2$): $p_4(x_2,t)$ is a solution of (4.4) with the boundary conditions:

$$p_4(x_2,t)\big|_{x_2=0} = A_{interface2}\sin(\omega t + \varphi_{inetrface2}), p_4(x_2,t)\big|_{x_2=L_2} = 0 \tag{4.22}$$

- Continuity condition for the interface between 3[d] and 4[th] zones is:

$$\frac{\partial}{\partial x_1} p_3(x_1,t)\Big|_{x_1=L_1} = \frac{\partial}{\partial x_2} p_4(x_2,t)\Big|_{x_2=0} \tag{4.23}$$

Similar to (4.19), (4.23) gives 2 scalar conditions: one for oscillation amplitude and one for oscillation phase.

Equations (4.19),(4.23) together with 6 conditions (4.16),(4.17),(4.18),(4.20),(4.21),(4.22) equating amplitudes and time lags in virtual sensors with those in real sensors E3, E4, G2 form a system of 10 scalar equations to determine the initial guess values for the parameters L_1, L_2, d_1, d_2, d_3, d_4, $A_{interface1}$, $\varphi_{interface1}$, $A_{interface2}$, $\varphi_{interface2}$.

After obtaining initial guess values, more accurate values of d_1, d_2, d_3, d_4 are found by running a series of numerical simulations as described in section 4.3, comparing the results with real sensor data and tuning the parameters.

4.6 Livedike diffusivities calibration

A training period of 48 hours has been used for diffusivities calibration. The following parameters values have been derived (Table 4-4):

Table 4-4. Calibrated values of diffusivities and homogeneous zones' lengths

(Horizontal diffusivity)·(water viscosity), Pa·m^2				**Zone length**	
$d_1 \cdot \mu$	$d_2 \cdot \mu$	$d_3 \cdot \mu$	$d_4 \cdot \mu$	L_1, m	L_2, m
$0.1 \cdot 10^{-3}$	$0.01 \cdot 10^{-3}$	$0.9 \cdot 10^{-3}$	$0.01 \cdot 10^{-3}$	82	13

Simulation results for a "training" period of two days are shown in Figure 4-15(a), for the E4 pressure sensor.

For long-term behaviour, slow attenuated fluctuations of the ground water level $h_{gw}(t)$ at the land side of the dike should be represented in the boundary condition. Month simulations for January 2010 and August 2009 periods have been performed. The attenuated signal $h_{gw}(t)$ has been obtained by averaging the tidal signal $h(t)$ with a one-day sliding window and multiplying it by a dissipation coefficient q: $h_{gw}(t) = q \cdot h(t)_{averaged}$ (see Figure 4-16 for January ground water table plot). The value of q varied depending on the season (q=0.15 for January and q=0.25 for August). Looking at Figure 4-16, we can see that the averaged tidal signal represents slow oscillations with the period varying between 2 and 3 days. Variation of the dissipation coefficient q with the season qualitatively agrees with the analytical solution (12) for propagation of slow fluctuations in homogeneous aquifer: according to (12), $q = e^{-x\sqrt{\frac{\pi}{Td}}} \Rightarrow$

$\Rightarrow q_{august} = e^{-(L_1+L_2)\sqrt{\frac{\pi}{Td}}} = 0.28$, where homogeneous aquifer diffusivity d=0.1 m^2/s, for slow oscillations with period T=48 hrs, aquifer length L_1+L_2=95 m;

$\Rightarrow q_{january} = e^{-(L_1+L_2)\sqrt{\frac{\pi}{Td}}} = 0.18$, for the aquifer with diffusivity d=0.1/1.8 m^2/s (which is summer diffusivity scaled by $\mu_{january} / \mu_{august}$), T=48 hrs, L_1+L_2=95 m.

Pore pressure fields for the high and low tides are shown in Figure 4-17. The unsaturated zone is shown with the white colour, so that the phreatic line is depicted as a boundary between white and coloured zones.

Fragments of the effective saturation field at the seaside are shown in Figure 4-18 for the high and low tides. During the low tide, water level inside the dike decreases and the sand located above the water table gets dry (yellow colour in Figure 4-18a). During the low tide the upper layer of clay, located above the water table, stays wet due to high water capacity of clay. In the high tide phase, water table rises and that can be seen in Figure 4-18b (blue saturated zone has enlarged, relatively to the Figure 4-18a).

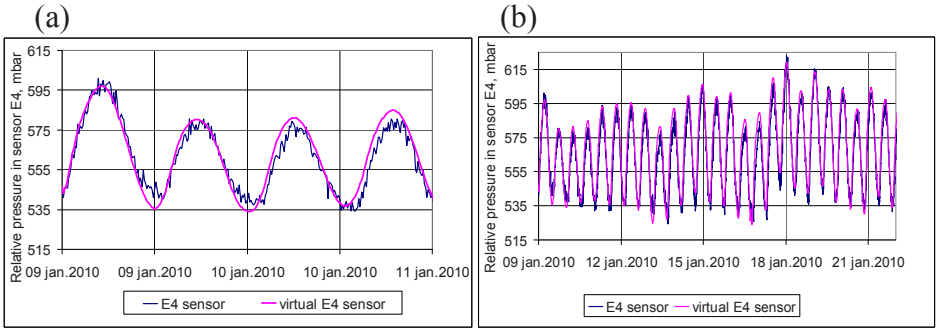

Figure 4-15. Relative pore pressure oscillations in sensor 1E4 with calibrated soil properties: (a) Comparison of real sensor data (blue) with simulation results (magenta) on training dataset; (b) The same, for a longer period of 12 days

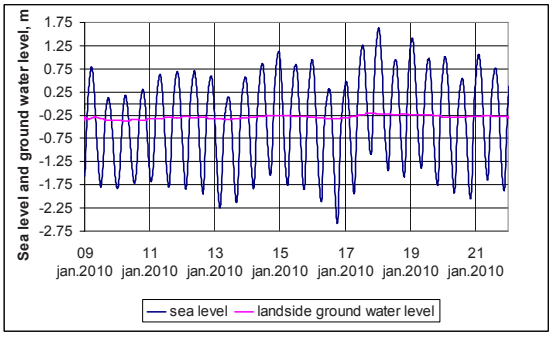

Figure 4-16. LiveDike calibration: sea level and attenuated ground water level at the land side boundary

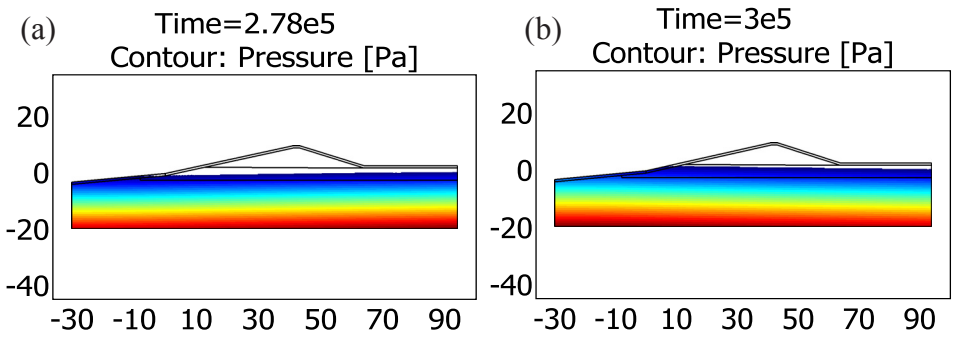

Figure 4-17. Pore pressure field: (a) low tide; (b) high tide

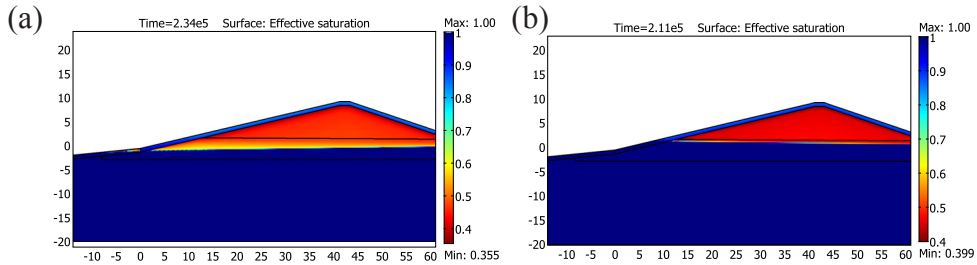

Figure 4-18. Effective saturation field: (a) low tide; (b) high tide

4.7 Conclusions

One of the scientific questions posed in this research was estimation of uncertainties influence on the dike stability assessment; it was important to find out how variations in soil properties alter dike safety margin.

We have focused on the influence of variation in soil diffusivity on the pore pressure distribution. Correct calculation of pore pressures in the dike is critical for the appropriate assessment of dike safety margin. Sensitivity analysis has shown that for coarse media (gravel, coarse sand), distribution of pore pressure amplitudes within a dike is close to linear and is defined by boundary conditions at the seaside and landside boundaries, while diffusivity value does not affect this distribution. For dense soils (fine sands, clays), pressure amplitudes distribution is highly non-linear and to a large extent depends on the diffusivity value.

On the base of these conclusions, we have constructed and implemented a new automatic procedure for calibration of soil diffusivities in an arbitrary heterogeneous dike based on historical pore pressure sensors recordings. The procedure has been successfully tested for the LiveDike diffusivities calibration: simulation results with calibrated soil parameters match experimental data, not only on the "training set" but also for a much longer period of time. The calibration procedure employs analytical solution obtained by us for the problem of tidal propagation in a one-dimensional finite homogeneous aquifer.